Journal of Neuroinflammation

RESEARCH

Open Access

Enhancing Th17 cells drainage through meningeal lymphatic vessels alleviate neuroinflammation after subarachnoid hemorrhage

Dandan Gao[1,3], Bin Zou[2,4], Kunyuan Zhu[1], Shijun Bi[1], Wenxu Zhang[1], Xinyu Yang[1], Jieyu Lai[1*], Guobiao Liang[1*] and Pengyu Pan[1*]

Abstract

Background Subarachnoid hemorrhage (SAH) is a severe cerebrovascular disorder primarily caused by the rupture of aneurysm, which results in a high mortality rate and consequently imposes a significant burden on society. The occurrence of SAH initiates an immune response that further exacerbates brain damage. The acute inflammatory reaction subsequent to SAH plays a crucial role in determining the prognosis. Th17 cells, a subset of T cells, are related to the brain injury following SAH, and it is unclear how Th17 cells are cleared in the brain. Meningeal lymphatic vessels are a newly discovered intracranial fluid transport system that has been shown to drain large molecules and immune cells to deep cervical lymph nodes. There is limited understanding of the role of the meningeal lymphatic system in SAH. The objective of this research is to explore the impact and underlying mechanism of drainage Th17 cells by meningeal lymphatics on SAH.

Methods Treatments to manipulate meningeal lymphatic function and the CCR7-CCL21 pathway were administered, including laser ablation, injection of VEGF-C geneknockout, and protein injection. Mouse behavior was assessed using the balance beam experiment and the modified Garcia scoring system. Flow cytometry, enzyme-linked immunosorbent assays (ELISA), and immunofluorescence staining were used to study the impact of meningeal lymphatic on SAH drainage. Select patients with unruptured and ruptured aneurysms in our hospital as the control group and the SAH group, with 7 cases in each group. Peripheral blood and cerebrospinal fluid (CSF) samples were assessed by ELISA and flow cytometry.

Results Mice with SAH showed substantial behavioral abnormalities and brain damage in which immune cells accumulated in the brain. Laser ablation of the meningeal lymphatic system or knockout of the CCR7 gene leads to Th17 cell aggregation in the meninges, resulting in a decreased neurological function score and increased levels

*Correspondence:
Jieyu Lai
BZLaijieyu@163.com
Guobiao Liang
liangguobiao6708@163.com
Pengyu Pan
panpengyu09@sina.com

Full list of author information is available at the end of the article

of inflammatory factors. Injection of VEGF-C or CCL21 protein promotes Th17 cell drainage to lymph nodes, an increased neurological function score, and decreased levels of inflammatory factors. Clinical blood and CSF results showed that inflammatory factors in SAH group were significantly increased. The number of Th17 cells in the SAH group was significantly higher than the control group. Clinical results confirmed Th17 cells aggravated the level of neuroinflammation after SAH.

Conclusion This study shows that improving the drainage of Th17 cells by meningeal lymphatics via the CCR7-CCL21 pathway can reduce brain damage and improve behavior in the SAH mouse model. This could lead to new treatment options for SAH.

Keywords Subarachnoid hemorrhage, Th17 cells, CCR7, CCL21, Meningeal lymphatic

Introduction

Subarachnoid hemorrhage (SAH) is a serious cerebrovascular accident that often ends in permanent neurological damage [1]. Early brain damage (EBI) occurs three days after the original injury, delayed cerebral ischemia (DCI) occurs three to four days later, and the peak incidence and severity happen six to eight days after the injury, according to the sequence of events following SAH [2]. The immune inflammatory process is also involved in brain damage after SAH. Interactions among immune cells populations, active compounds, and inflammatory responses exacerbate SAH symptoms and worsen the prognosis. The inflammatory response of immune cells is a crucial physiological mechanism that occurs after SAH [3, 4]. However, the mechanism of immune cell clearing is still unclear.

SAH-induced inflammation activates NK cells, B cells, neutrophils, and T cells. These cells trigger immunological responses and inflammatory processes via secreting cytokines, inflammatory mediators, and reactive oxygen species [5–7]. $CD4^+$ lymphocytes, a type of T lymphocyte, play a vital role in inflammatory reaction that occur after SAH. Studies indicate that CD4 cells can be classified as Th1, Th2, Th17, and Treg subsets, each playing a different role in the inflammatory reaction after SAH [8]. Pro-inflammatory substances are released during the early phases of SAH due to Th1 and Th17 cell activation, which intensifies the inflammatory cascade [9]. Th17 cells, a specific subtype of $CD4^+$ T cells, are instrumental in the initiation of early tissue inflammation, a characteristic feature of numerous immune-inflammatory diseases. Th17 cells and inflammatory mediators like IL-17 are markedly increased in the brain after bleeding [10]. IL-17 after SAH can worsen initial brain damage by increasing blood-brain barrier (BBB) breakdown, leading to cerebral swelling, and enhancing apoptosis and neuronal death [11]. Following SAH, the immune response involves a variety of immune cells. It has been found that meningeal lymphatic vessels can discharge immune cells entering deep cervical lymph nodes (dCLNs) from cerebrospinal fluid (CSF) in the central nervous system (CNS).

Immune cells were supposed to migrate via the meningeal lymphatic system by the CCR7-CCL21 pathway [12]. CCR7 serves as a chemokine receptor, while CCL21 functions as a chemokine. Their interaction with the meningeal lymphatic system initiates a signaling interaction that directs the movement of immune cells. Immune cells expressing CCR7 exhibit the capability to adhere to CCL21 present on the meningeal lymphatic system, facilitating their migration along these vessels towards the cervical lymph nodes. To dissect the role of meningeal lymphatics in SAH, we used a mouse model to investigate the potential mechanism of the CCR7-CCL21 pathway in draining Th17 cells. Our research findings provide a basis for further research and development of meningeal lymphatic regulation therapy for secondary brain tissue injury caused by SAH.

Materials and methods

Experimental subjects

202 wild-type male C57BL/6 mice, 76 male Flox mice, and 38 male CCR7knockout (KO) mice weighing approximately 24 g were used in this experiment. These animals were from the Northern Theater Hospital's Laboratory Animal Center. The clinical patient samples were selected from patients who were admitted to our hospital from June 1, 2023, to December 1, 2023, including a total of 14 patients, 7 cases in each of the SAH and control groups.

Experimental design

The experiment was structured into five distinct sections, as illustrated in Fig. 1.

The initial phase involved the selection of sham and SAH groups at (12 h, 24 h, 2d, and 3d), with enzyme-linked immunosorbent assays (ELISA) utilized to measure IL-17 levels alongside assessments of neurological function scores. The time curve of IL-17 and neurological function score was described after SAH.

The following part was to find out how Th17 cells affect SAH. Four groups were divided to investigate the impact of Th17 cells on SAH: sham, Vehicle, Th17 cells, and Anti-IL-17 group. IL-17 antibodies and Th17 cells were

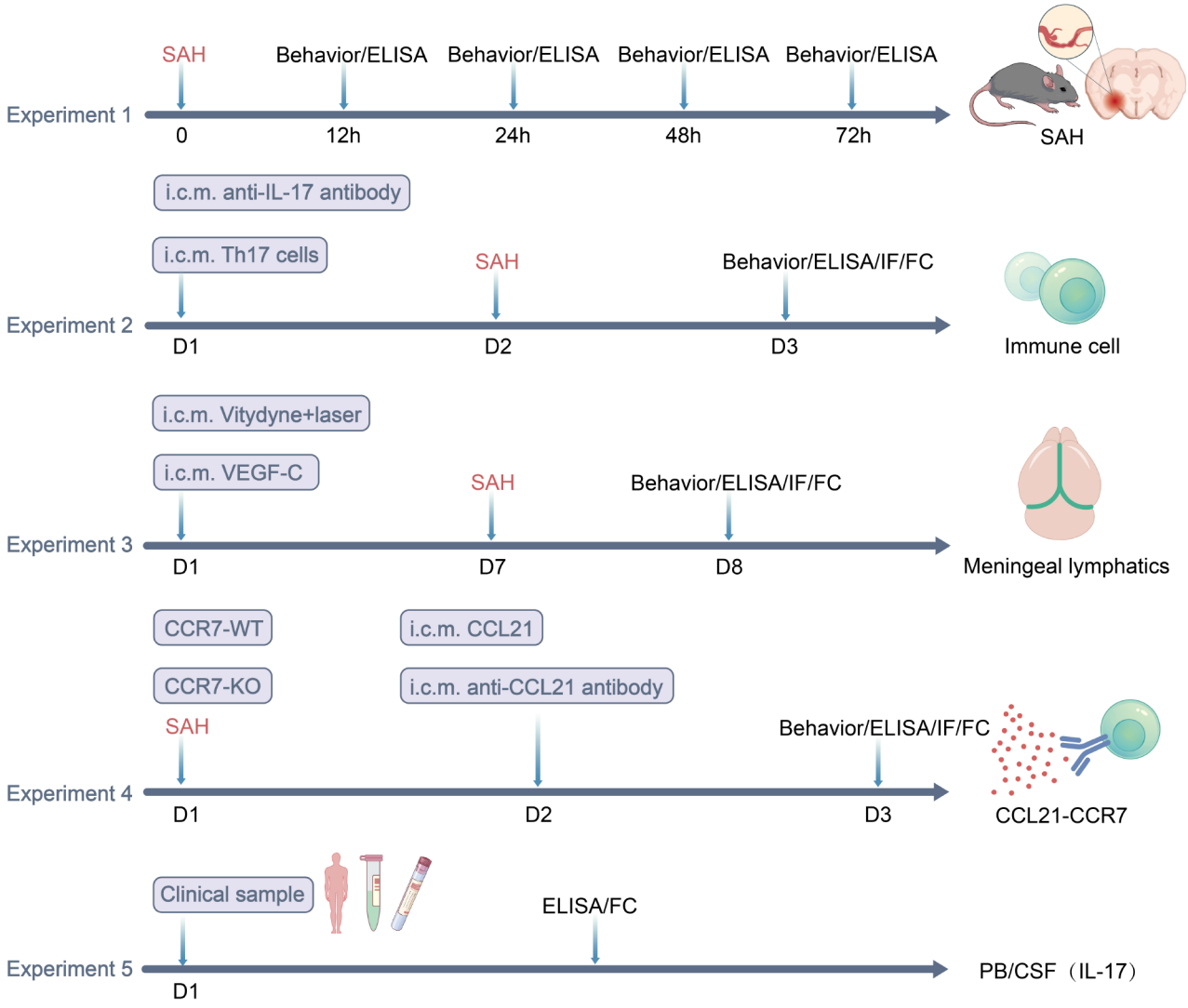

Fig. 1 Flowchart of this experiment

injected into the cisterna magna. ELISA, immunofluorescence, and flow cytometry were included.

In the third section of the study, we investigated the effects of meningeal lymphatic drainage on Th17 cells. VEGF-C, Visudyne, and laser ablation were used to intervene in the meningeal lymphatic drainage. The study included sham, Vehicle, L(laser)+SAH, L(laser)+V(Visudyne)+SAH, and VEGF-C+SAH groups.

The fourth section of the study focused on investigating the CCR7-CCL21 pathway on immune cell drainage within the meningeal lymphatic system. We knock out the CCR7 gene and inject CCL21 antibody/CCL21 protein to regulate the CCR7-CCL21 pathway in the meningeal lymphatic system. Six groups were included in the study: sham, Vehicle, CCL21, Anti-CCL21, KO+CCL21, and KO+Anti-CCL21. Mice in the sham, Vehicle, CCL21, and Anti-CCL21groups were all Flox mice.

In the fifth section of the study, the control group consisted of patients with unruptured aneurysms, while ruptured aneurysms were in the SAH group from our hospital, with 7 cases in each group. ELISA was utilized to assess the levels of inflammatory factors in samples of peripheral blood and CSF. Flow cytometry was used to evaluate the Th17 cell levels.

Mouse SAH model

Endovascular perforation surgery was used to cause SAH in mice [13]. The mice were injected with 1% pentobarbital sodium intraperitoneally at a dosage of 50 mg/kg, and surgery was performed under a surgical microscope. A midline incision was made in the neck to access. After being located, transversely cut the external carotid artery

to the distal end to form a 2 mm stump. A 5−0 sharp single -threaded nylon suture was pushed through the internal carotid artery into the internal carotid artery until resistance was encountered, then further pushing the suture 2 mm to enter the bifurcation of the anterior and middle cerebral arteries. The internal carotid artery was reperfusion to form SAH, and the suture was removed. The identical technique was performed on sham-operated mice, but after experiencing resistance, the suture was removed without puncturing the cerebral artery.

Behavioral scoring

The assessment of neurological impairments was estimated 24 h following SAH induction, utilizing the modified Garcia scale [13]. This encompasses six components: spontaneous activity, forelimb extension capability, climbing proficiency, body reflexes, and whisker touch responsiveness. Three factors contribute to the balance beam score, with each factor having a value between 0 and 3, for a total score that can span the range of 3 to 18. A higher score was indicative of improved brain function. To calculate the balance beam score, a rectangular crossbar measuring 90 cm in length and 1 cm in width was positioned between two plates of approximately 10 cm^2 in size. During the experiment, mice were placed on the plates for 10 s each, followed by observation of their movement on the crossbar for 40 s. A higher score denotes improved neurological function. Scores were given on a scale of 0 to 5. Each experiment was conducted by two double-blind experimenters.

Measurement of brain water content

Based on previously published protocols [13], the wet weight was determined and documented using an analytical balance. The brain tissue was then subjected to a 24-hour period in an electric oven set at 105 °C. The dry weight was subsequently employed to compute the water content. The percentage of water content in the brain can be calculated using the formula [(wet weight - dry weight) / wet weight] × 100%.

Intra-cisterna magna injection

After injecting 1% pentobarbital sodium into the mouse's abdominal cavity, we placed the mouse in a prone position and created an angle of approximately 120° between its head and trunk. Shave off the hair on the back of the mouse's neck, disinfected with 75% alcohol, and make a midline incision to expose the posterior atlantooccipital membrane. Fixed the head of the mouse delicately while holding a 5μL microsyringe and inserting the needle down the center of the neck at a 45° angle, a palpable pop felt when the needle entered subarachnoid space, advanced the needle at a depth of 4 mm. Administered the solution slowly at 0.1μL/min. The needle should be kept in place for 30 s prior to its removal. The contents administered into the cisterna magna in this experiment include Th17 cells (1 million total in 2μL), IL-17 antibody 2μL (Invitrogen), Visudyne 5μL (Aladdin), VEGF-C 5μL (Novoprotein), CCL21 antibody 2μL (Bioss), and CCL21 protein 2μL (MCE).

Visudyne treatment

Previous research has demonstrated that meningeal lymphatics can be destroyed through cisterna magna injections and transcranial photoconversion using Visudyne [14]. The mouse was injected with 1% pentobarbital sodium intraperitoneally at a dose of 50 mg/kg. 15 min after Visudyne injection, a nonthermal laser from the 689 nm wavelength was utilized to focus on the junction of the left and right transverse sinuses, superior sagittal sinuses, and all sinuses. The laser was applied for 83 s with a dose of 50 J/cm^2 and a power of 600 mW/cm^2. The mice were placed on a warming pad until they woke up. Mice treated with Visudyne and Vehicle group underwent SAH induction on day 7 after the procedure.

Th17 cells sorting

The euthanasia of a mouse ($n=1$) was conducted via abdominal injection of 1% pentobarbital sodium intraperitoneally at a dose of 50 mg/kg. Following this, spleen tissue was removed, ground, and processed into a single-cell suspension by passing it through a 70-mesh cell strainer and sterile plunger. The suspension was mixed with red blood cell lysis solution and cooled on ice for 15 min, then vortexed twice. The phycoerythrin (PE)-conjugated anti-CD4 antibody (1:200, TONBO Biosciences) and PE-conjugated anti-CD161 antibody (1:200, TONBO Biosciences) were used for the identification of Th17 cells. The suspension was subsequently sorted using a BD flow cytometer, resulting in CD161 expression levels of 80% on the sorted cells, indicating successful isolation of Th17 cells [15].

Th17 cells tracking

Prior to injection, the cells were stained with Deep Red Dye (Thermo Fisher), following the guidelines provided by the manufacturer. CellTracker™ Deep Red dye was diluted to reach the final working concentration of 0.5–25 μM in serum-free medium. The CellTracker™ Working Solution should be warmed to 37 °C. Flow cytometry sorted Th17 cells were added to a culture medium, containing dyes. Incubated in a 37 °C oven for 30 min. Centrifuged cells, added the selected culture medium and allocated labeled cells. Injected labeled cells into the occipital cistern of mice and took meninges for confocal imaging [16].

Immunofluorescence

After administering 1% pentobarbital sodium to induce full anesthesia in mice, perfused mice with PBS and 4% paraformaldehyde (PFA) at 24 h after SAH. The brains were quickly removed, then fixed and dehydrated in 4% PFA solution and 30% sucrose solution. The dehydrated brain tissue was embedded in medium and sectioned using a cryostat at -34 °C with a thickness of 6 μm. Subsequently, they underwent three 10-minute washes with 1×PBS to wash off the medium and then incubated for 60 min in a humidified chamber with a blocking solution. Following the addition of primary antibodies, incubated the mixture overnight at 4 °C. Anti-Lyve-1 antibody (1:200, Invitrogen), anti-VEGFR3 antibody (1:200, Bioss), anti-CD4 PE conjugated antibody (1:200, TONBO Biosciences), anti-IL-17 fluorescein isothiocyanate (FITC) conjugated antibody (1:200, Invitrogen), anti-IL-17 Alexa Fluor 647 conjugated antibody (1:200, Invitrogen), anti-CCR7 antibody (1:200, Bioss), and anti-CCL21 antibody (1:200, Bioss) were the primary antibodies used for immunofluorescence analysis. The tissue slices were then subjected to three 10-minute washes with 1×PBS, secondary antibody addition, and a 1-hour incubation period in a humidified, dark environment. The secondary antibodies used were Alexa Fluor 555 goat anti-rabbit and Alexa Fluor 488 goat anti-mouse antibodies (1:200, Bioss). The slices were mounted with DAPI-containing media after three additional 10-minute washes with 1×PBS. Fluorescence microscopy and confocal laser microscopy were used to observe and capture images [16].

ELISA

The brain tissue from the ipsilateral injured hemisphere was homogenized using an appropriate amount of normal saline (saline: brain tissue=9 ml:1 g). The mixture was then centrifuged at 3000 rpm for 10 min at 4 °C to obtain the supernatant. The ELISA procedure adhered to the guidelines provided by IL-17 manufacturer (Neobioscience) reagent kits. Prior to use, the reagents were equilibrated to room temperature. The lyophilized standard sample was reconstituted by adding IL-17 to 0.5 mL of universal diluent and allowed to dissolve completely over a 15-minute incubation period. The resulting solution was gently mixed to achieve a concentration of 1000 pg/mL. A standard curve was constructed using concentrations ranging from 0 to 1000 pg/mL. Empty wells were filled with standard and sample diluent, while the remaining wells were filled with specimens or varying concentrations of standards (100 μL each). Following a 90-minute incubation in the dark, the plate was rinsed five times. The first well was treated with biotinylated antibody diluent, while the remaining wells received 100 μL of the working solution. After 60 min of incubation, the plate went through five rounds of washing. The blank wells were diluted with enzyme conjugate diluent, while the remaining wells received 100 μL of the working solution. The reaction wells were sealed with fresh tape and then incubated at 37 °C for 30 min without light. The plate underwent an additional five washes before the results were recorded. After adding 100 μL of chromogenic substrate to every single well, incubated for 15 min at 37 °C without light. Next, add 100 μL of the reactivity termination solution to all of them well and mix thoroughly. An optical density at the wavelength of 450 nm (OD450) was subsequently measured. Other inflammatory factors were detected using ELISA [12].

Flow cytometry

Mouse brain tissue was removed and processed in a tissue grinder with PBS at 4 °C. To achieve an ending volume of 7 mL, the homogenate was passed through a 70-mesh filter and mixed with 0.01 M PBS. Subsequently, 3 mL of de-cluttering working solution was added to the mixture in a 7:3 volume ratio, followed by gentle mixing. The mixture had been centrifuged for a period of 15 min at 4 °C and 450 g, and the supernatant was extracted. After removing the residual supernatant, the cells were then suspended in 500–1000 μL of pre-cooled 1×PBS buffer. Rinse cells with cooled 1×PBS buffer, whirled for a period of five minutes at 300 g, and collected the supernatant. The cells were then counted under a microscope after being reconstituted in 500–1000 μL of PBS buffer.

To harvest meningeal lymphatic vessels, a fully intact mouse dura mater of calvarium post-perfusion was removed. Subsequently, the dura mater was meticulously dissected under a microscope. Following this, the dura mater was immersed in DMEM solution supplemented with 1 mg/mL DNAse and 1.4 U/mL collagenase. The resulting mixture underwent incubation at 37 °C for a duration of 15 min, then stirred, filtration through a 70-mesh filter, and centrifugation at 450 g for 15 min. After the supernatant was aspirated, the dura mater cells were resuspended in PBS buffer and used for the following experiments.

For process lymph nodes, a longitudinal incision from mandible to sternum allowed access to dCLNs, which were located beneath the lower section of the sternocleidomastoid muscle. The dCLNs were then separated in DMEM that had 10% fetal bovine serum added to it. The meninges, fragmented brains, and dCLNs were then isolated and filtered through a 70-mesh sieve.

The cell suspension was incubated with CD4 antibody at 4 °C for 30 min. A BD Biosciences flow cytometer was used to collect the data, and FlowJo (version 10.6.2) was used for analysis. The number of Th17 cells in each brain, meninge, and dCLNs was calculated. For preparation of single-cell suspensions, the mice were perfused

with a pre-cooled 0.01 M PBS solution, and tissue was collected. The anti-CD4 antibody conjugated with PE (1:200, TONBO Biosciences) and an anti-IL-17 antibody coupled with FITC (1:200, TONBO Biosciences). For each analysis, 5000 cells were used for meningeal samples, while 20,000 cells were utilized for brain and dCLNs samples [12].

Data statistics and analysis

The study's data were shown as mean±SD. A one-way analysis of variance (ANOVA) was performed, followed by a Tukey's multiple comparisons test to compare different groups. An independent sample t-test for two groups of clinical samples to compare, $P<0.05$ for statistical significance. GraphpadPrism 9.5 was applied for data analysis and graphical representation.

Results

The Th17 cell levels increase after 24 h of SAH

The most notable outcome was observed 24 h after SAH and demonstrated statistical significance when compared to the sham group. The Garcia and balance beam investigations revealed a significant ($P<0.05$) drop in results at the 24-hour post-SAH time point, as shown in (Fig. 2). This suggests that the most severe neurological impairment and brain edema occur 24 h following SAH, and 24 h was chosen for further experiment. The Th17 cell group had significantly worse Garcia and balance beam neurological function scores than the Vehicle group. Conversely, the Anti-IL-17 group showed superior performance compared to the ehicle group, as illustrated in (Fig. 3A, B). This experiment assessed the water content of three independent brain areas: left hemisphere, right hemisphere and cerebellum. When compared to the Vehicle group, The Th17 cells group had the highest brain water concentration. Conversely, the Anti-IL-17 group exhibited reduced brain water content compared to the Vehicle group. This suggests that Th17 cells aggravate brain damage and edema following SAH (Fig. 3C). Inflammatory cytokines were more elevated in the Th17 cell group compared to the Anti-IL-17 and Vehicle SAH groups. These findings suggest that SAH produces inflammatory damage, while Th17 cell infusions exacerbate this damage. On the other hand, injecting antibodies has the potential to minimize inflammatory effects (Fig. 3D-F). Immunohistochemical analysis of brain slices showed that the Vehicle group exhibited elevated levels of CD4 and IL-17 compared to sham group (Fig. 3G), whereas the Th17 cell group had higher IL-17 levels than the Anti-IL-17 group. Flow cytometry analysis showed that the Th17 cells group had a greater percentage of Th17 cells compared to the Vehicle and sham groups. (Fig. 3H, I) The foregoing findings suggest that Th17 cells increase brain damage following SAH.

Th17 cells accumulated in brain are drained by the meningeal lymphatics to dCLNs

Meningeal drainage was altered by Visudyne and laser ablation, which effectively blocked meningeal lymphatic drainage. After injecting sorted Th17 cells labeled with cell trackers into the cisterna magna, labeled Th17 cells can be found in the transverse sinus (Fig. 4A). Meningeal lymphatics in the L+V+SAH group were discontinuous, whereas VEGF-C encouraged the enlargement of transverse sinuses (Fig. 4B). CD4 levels increased in Vehicles as shown in (Fig. 4C). VEGF-C protein was injected into the cisterna magna to improve meningeal lymphatic function. The L+V+SAH group scored the lowest on the Garcia and balance beam neurological function tests, lower than the Vehicle group. Conversely, the Anti-IL-17

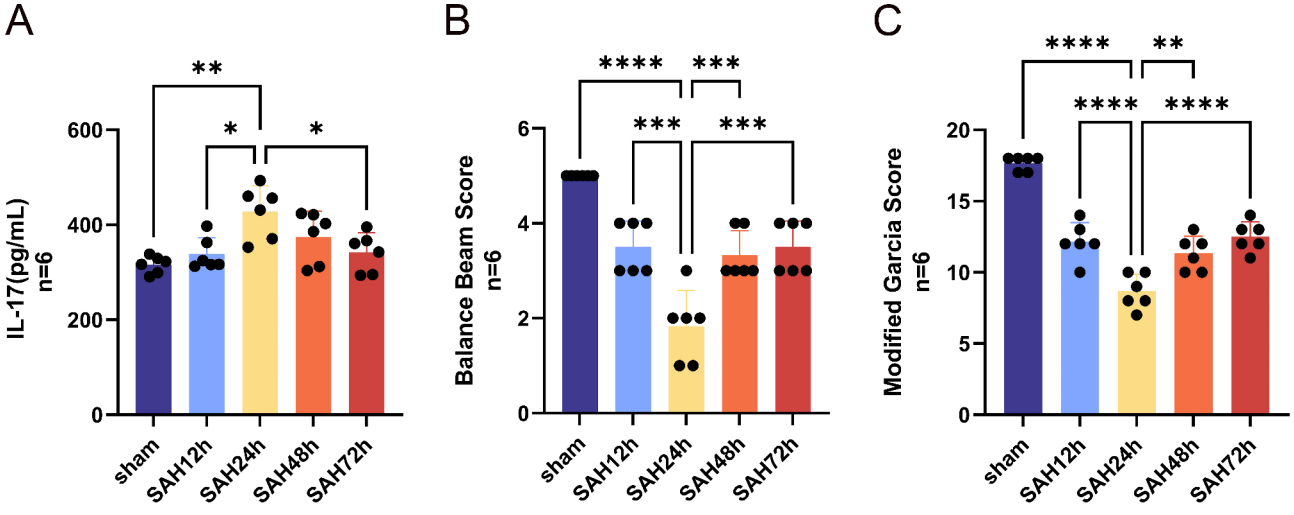

Fig. 2 The development of IL-17 cytokine levels in early brain injury following SAH, as well as neurologic function ratings. **A** Time curve of IL-17 assayed by ELISA. **B**, **C** The Garcia and balance beam scores, *$P<0.05$, **$P<0.01$, ***$P<0.001$, ****$P<0.0001$. ns, not significant

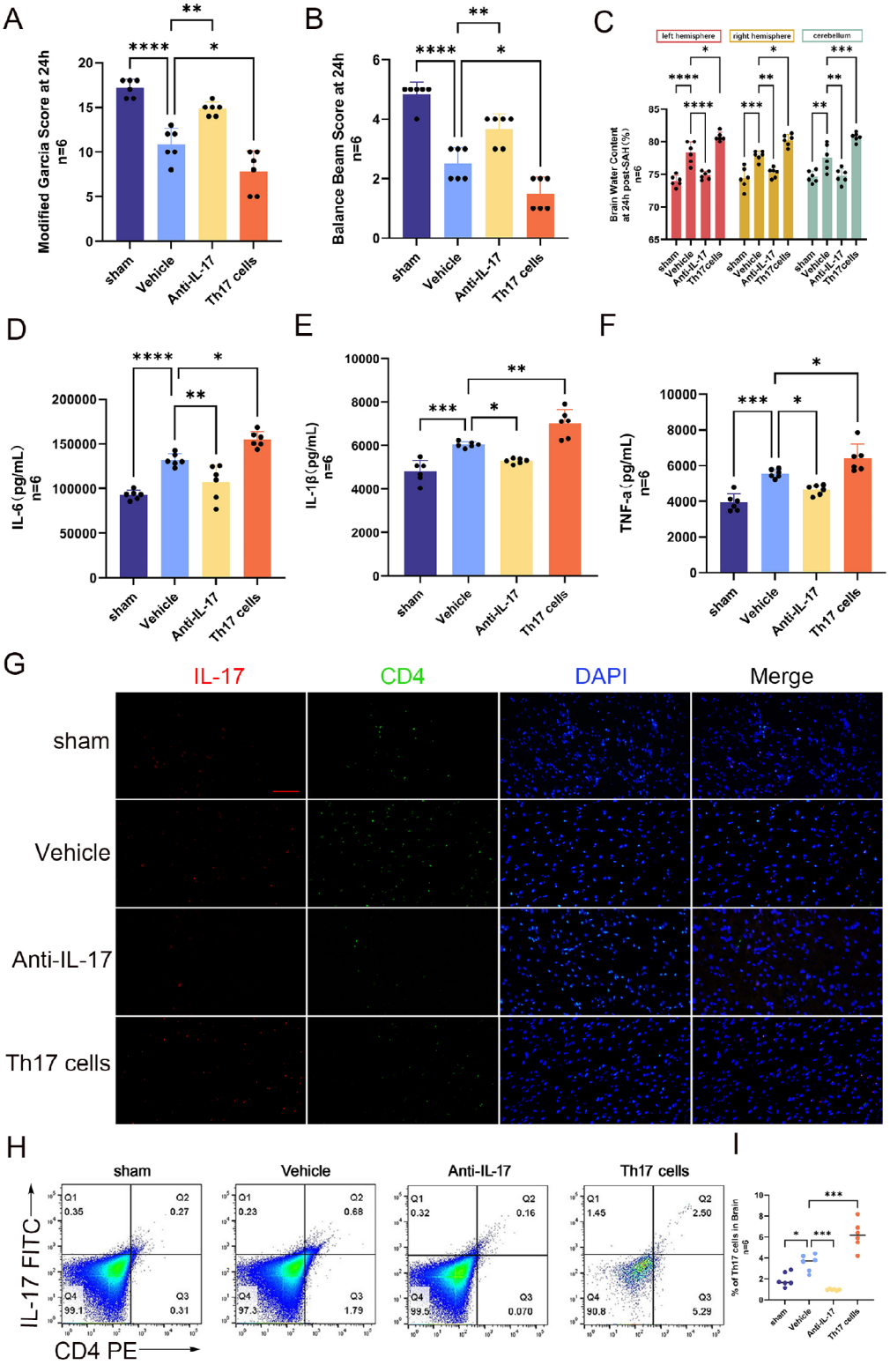

Fig. 3 Th17 cells following SAH worsen brain damage, edema, and the neuroinflammatory response. **A**, **B** neurological function score from the Garcia test and balance beam test. **C** After SAH, the Th17 cell group showed significantly higher brain water content than the Vehicle group ($P < 0.05$). **D-F** ELISA measurements of IL-6, IL-1β, and TNF-a levels. ($P < 0.05$). **G** Immunofluorescence labeling of CD4 and IL-17 in each group (IL-17 red, CD4 green, DAPI blue, scale bar = 50 μm, $n = 1$). **H** Flow cytometry study of Th17 cell counts in brain tissue. Statistical analysis of Th17 cell numbers in each group. **I** Statistical study of each group's Th17 cell numbers, *$P < 0.05$, **$P < 0.01$, ***$P < 0.001$, ****$P < 0.0001$. ns, not significant

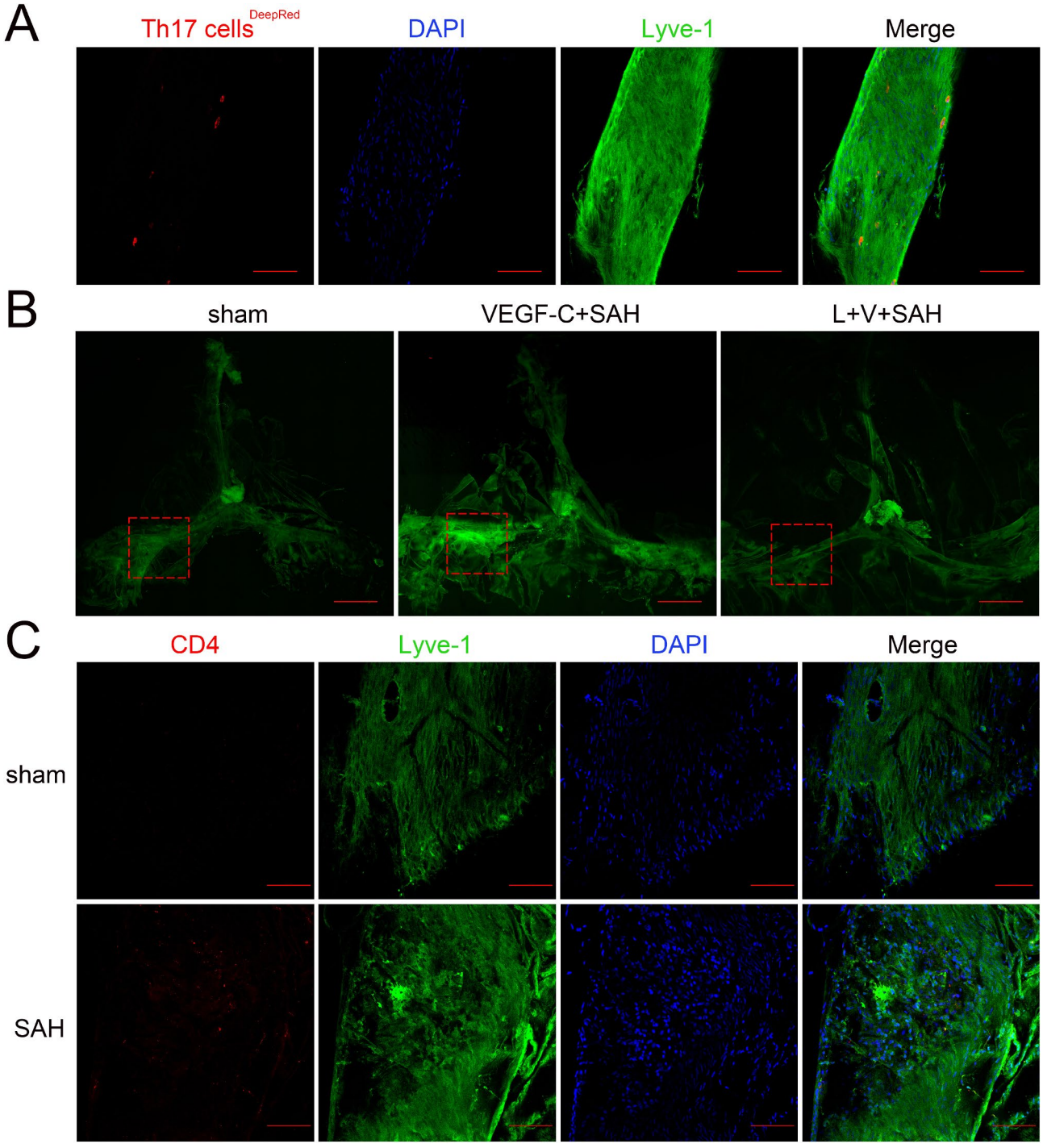

Fig. 4 Ablation of meningeal lymphatic vessels and Th17 cells tracking. **A** Representative confocal imaging of the transverse sinus after injection of Th17 cells with tracking dye into the occipital cistern (Lyve-1 green, Th17 cells red, DAPI blue, scale bar = 100 μm, $n = 1$). **B** Imaging of meningeal lymphatic vessels after laser ablation, Visudyne + laser ablation, and VEGF-C injection in the L + V + SAH group, the transverse sinus is intermittently discontinuous, whereas in the VEGF-C group, it is substantially thicker (Lyve-1 green, scale bar = 1000 μm, $n = 1$). **C** Local CD4 + Lyve-1 imaging of the superior sagittal sinus in the sham and SAH groups (Lyve-1 green, CD4 red, DAPI blue, scale bar = 100 μm, $n = 1$)

group had superior performance compared to the Vehicle group (Fig. 5A, B). The L + V + SAH group had the largest brain water content, indicating that L + V aggravates brain injury and edema, whereas VEGF-C decreases brain injury and edema (Fig. 5C). ELISA results indicated that the L + V + SAH group showed elevated levels of inflammatory cytokines in comparison to the remaining groups. Significant differences were observed between

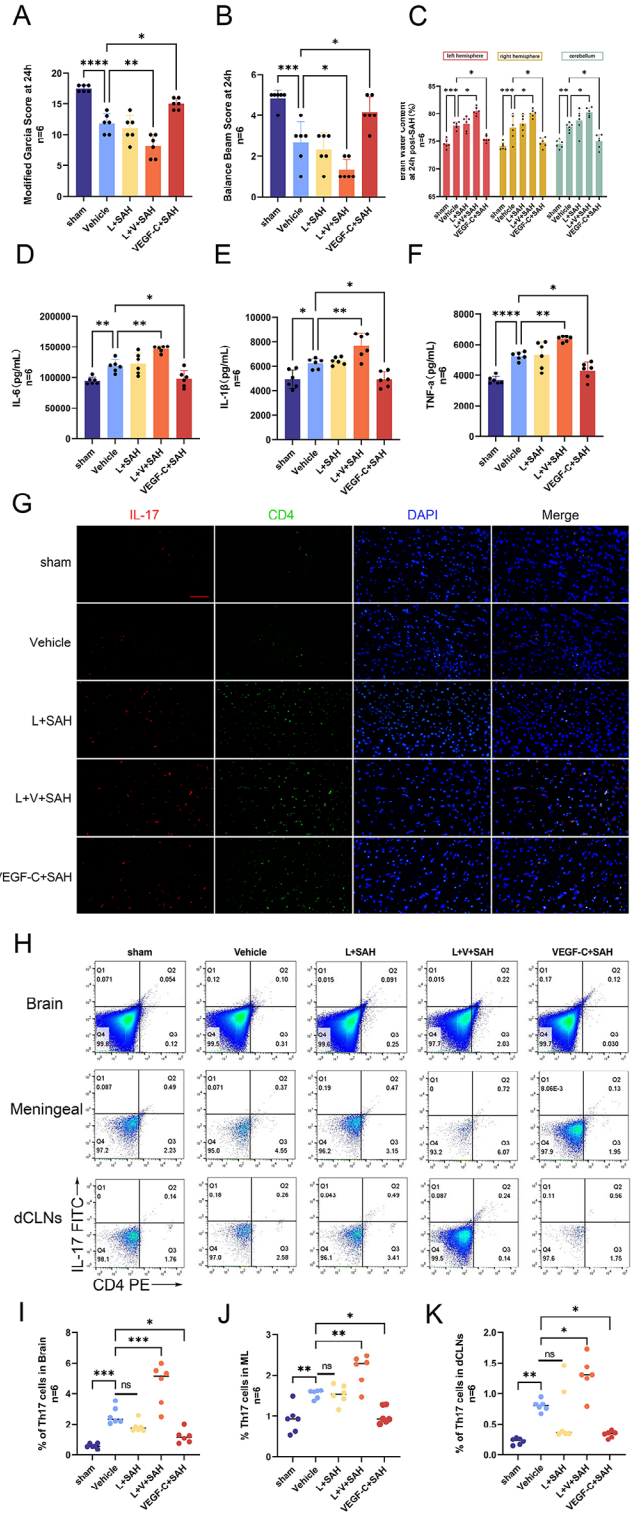

Fig. 5 Ablation of meningeal lymphatics aggravates brain damage, edema, and the neuroinflammatory response in SAH. **A** Garcia test **B** balance beam test. **C** Measurement of brain water content following SAH. The L + V + SAH group had the highest brain water content. **D-F** Levels of IL-6, IL-1β, and TNF-a were determined by ELISA. **G** Immunofluorescence revealed that CD4 and IL-17 levels were higher in the L + V + SAH group than in the Vehicle group but lower in the VEGF-C group (IL-17 red, CD4 green, and DAPI blue; scale bar = 50 μm, $n = 1$). **H** Th17 cell counts in brain tissue, meningeal lymphatics, and dCLNs were analyzed using flow cytometry. **I-K** Statistical study of each group's Th17 cell numbers, *$P < 0.05$, **$P < 0.01$, ***$P < 0.001$, ****$P < 0.0001$. ns, not significant

the Vehicle and VEGF-C groups, as shown (Fig. 5D-F). Using fluorescence microscopy, brain tissue sections from the L+V+SAH group revealed more immune cells than those from the VEGF-C group (Fig. 5G). Flow cytometry analysis revealed Th17 cells fewer in dCLNs in the L+V+SAH group (Fig. 5H-K). Disruption of the meningeal lymphatic pathway blocked cells from reaching the dCLNs. In contrast, the VEGF-C group had more Th17 cells in their dCLNs.

The interaction between CCR7 and CCL21 facilitates Th17 cell drainage via the meningeal lymphatic system

Sham and the Vehicle group's meningeal lymphatics expressed both CCR7 and CCL21; CCR7 and CCL21 levels slightly increased in the Vehicle group (Fig. 6A). The KO group exhibited increased IL-17 staining compared to the Flox group, with IL-17 expression observed in the meninges of the Flox group (Fig. 6B). The CCR7-KO group's neurological function scores fell, and the Anti-CCL21 group fared worse than the CCL21 group (Fig. 7A-B). Analysis demonstrated that the KO+CCL21 and KO+Anti-CCL21 groups had similar brain water content levels, with no statistically significant differences. Moreover, a significant variance was observed between the Anti-CCL21 and Vehicle groups. Brain water content was shown to be lower in the CCL21 group, but higher in KO+CCL21 than CCL21 group. Furthermore, it shows that the KO+Anti-CCL21 group had more brain water than the Anti-CCL21 group (Fig. 7C). This suggests that the CCR7-KO group experienced significant brain injury and edema, but the CCR7-KO group received an injection of CCL21 antibody, which exacerbated brain injury and edema levels, while the injection of CCL21 protein reduced brain injury and edema. ELISA results showed the KO+CCL21 and KO+Anti-CCL21 groups did not differ significantly from one another. Cytokine levels were significantly lower in the CCL21 group but significantly higher in the Anti-CCL21 group (Fig. 7D-F). KO+CCL21 group exhibited in comparison to both CCL21 group and KO+Anti-CCL21 group, which showed higher levels than Anti-CCL21 group (both with $P<0.05$). It was found that the Vehicle group exhibited IL-17 and CD4 higher than the sham group. The Anti-CCL21 group exhibited higher than the Vehicle group. The CCL21 group exhibited notably reduced levels of IL-17 and CD4. Moreover, the levels were notably higher in the CCR7-KO group that received Anti-CCL21 and CCL21 treatment (Fig. 7G). There was no difference in Th17 cell counts between the KO+CCL21 and KO+Anti-CCL21 groups, as determined by flow cytometry of brain tissue homogenates and meningeal samples. It is worth noting that Th17 cell numbers were much lower in the CCL21 group than the Vehicle group but significantly higher in the Anti-CCL21 group (Fig. 7H). Th17 cell counts between the KO+CCL21 and KO+Anti-CCL21 groups showed no difference. Obviously, Th17 cell numbers were much lower in CCL21 than in the Vehicle group but significantly higher in the Anti-CCL21 group (Fig. 7I-K).

The inflammatory factors in the SAH group were higher than the control group in clinical specimens

Inflammatory cytokines levels in blood and CSF of SAH patients significantly increased, and it has statistical significance. (Fig. 8A–C). Statistical analysis revealed higher concentrations of all three cytokines in CSF samples from the SAH group. (Figure. 8G-H), IL-17 levels with SAH were notably elevated. SAH group displayed notably higher Th17 cell levels in both blood and CSF ($P<0.05$). The above results indicate that early neuroinflammatory damage following SAH is higher than in the control group.

Discussion

SAH is a commonly occurring acute disease that is usually caused by the rupture of aneurysms or other vascular abnormalities located inside the subarachnoid space [17]. Additionally, the human immune system is considered to play a vital role in the pathophysiological processes of SAH [18]. EBI occurs within 72 h of SAH. EBI is characterized by elevated intracranial pressure (ICP), reduced cerebral blood flow (CBF) and cerebral perfusion pressure (CPP), BBB breakdown, oxidative stress, and inflammation [19, 20]. Comprehending the role of immune cells after SAH is crucial for devising successful treatment approaches. CD4 cells are implicated in the onset of neuroinflammatory disorders, such as experimental autoimmune encephalomyelitis, and the possible mechanisms are as follows: in some cases, persistent contact was established between CD4 cells and major histocompatibility antigen MHC class II positive antigen-presenting cells. However, there has been limited research on the role of immune cells in SAH [21]. According to Samuel X. Shi's research, $CD4^+$ T cells that have been activated during intracerebral hemorrhage gather in the perihematomal area and cause local inflammation by producing IL-17 and binding to endothelial cell death receptors. This will reduce the integrity of the BBB and increase brain edema [15]. We have determined that T cell-mediated immunity plays a role in the early rupture of aneurysms [22]. The rupture of an aneurysm can result in SAH, which can trigger both innate and adaptive immune responses [23]. The innate immune cells in the circulatory system quickly participate at the beginning of aneurysm rupture, leading to the brain parenchyma experiencing significant infiltration of blood- derived immune cells, which consequently activates the inherent immune cells within the brain. Adaptive immunity is mediated by diverse T cell receptors present on the surface of T

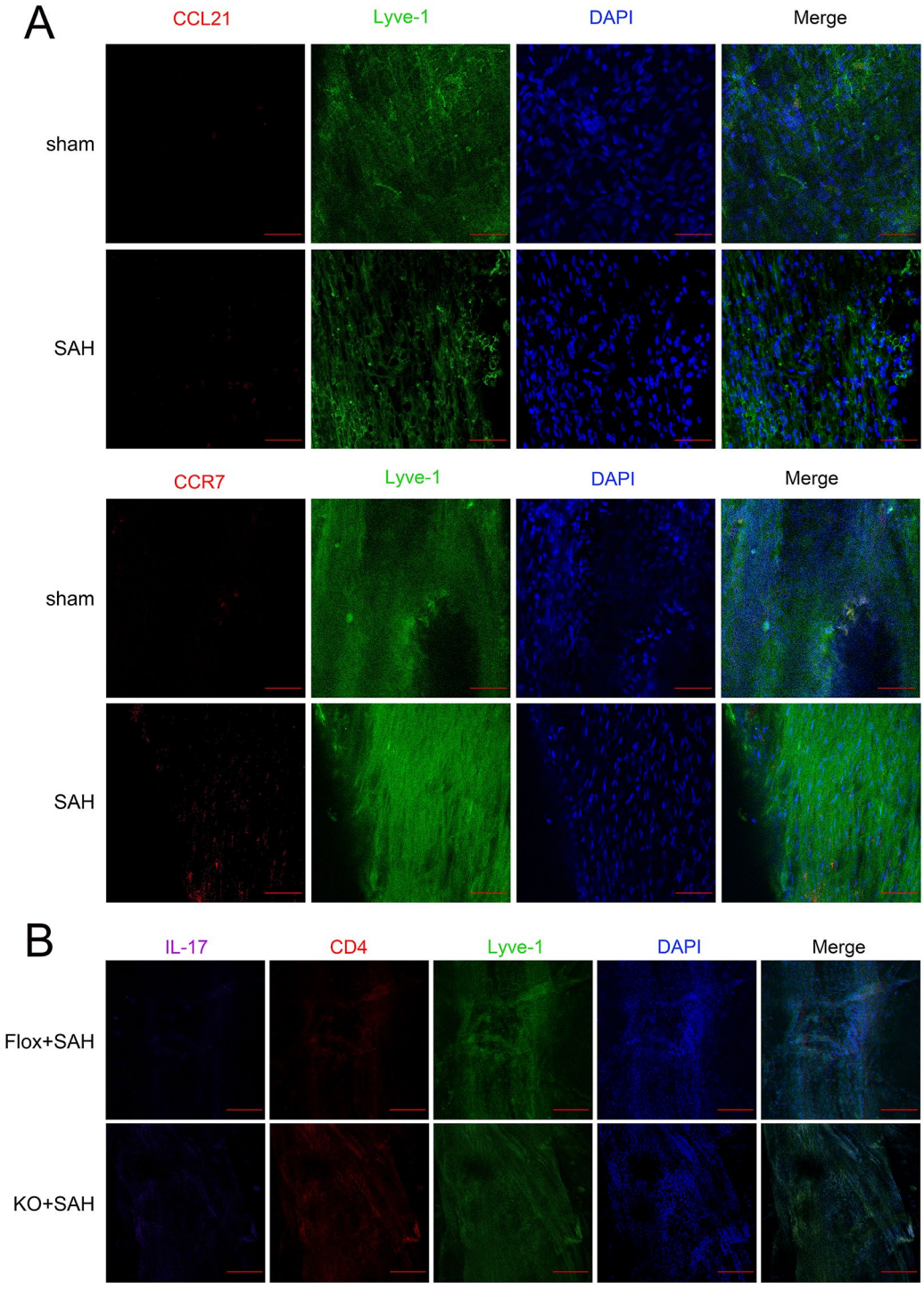

Fig. 6 Flox and CCR7-KO group of meningeal lymphatic vessels. **A** Representative confocal images of CCR7 and CCL21 in the meninges of the sham and SAH group (CCR7 and CCL21 red, Lyve-1 green, DAPI blue, scale bar = 100 μm, $n = 1$). **B** Representative confocal images of expression of IL-17, CD4, and Lyve-1 in the meninges of the Flox group and the KO group. Compared to the Flox group, Th17 cells were increased in the KO group (IL-17 purple, CD4 red, Lyve-1 green, DAPI blue, scale bar = 250 μm, $n = 1$)

lymphocytes, which recognize pathogens and monitor the host's immune response [24]. In addition, according to the infiltration of lymphocytes in the arteries, lymphocytes participate in the pathophysiology of SAH. Besides, $CD4^+$ T lymphocyte infiltration is high and reaches peak levels in early SAH models [25]. In addition, in a clinical study, a notable rise in Th17 cells and a reduction in Th2 cells were detected following SAH [26]. Ischemic

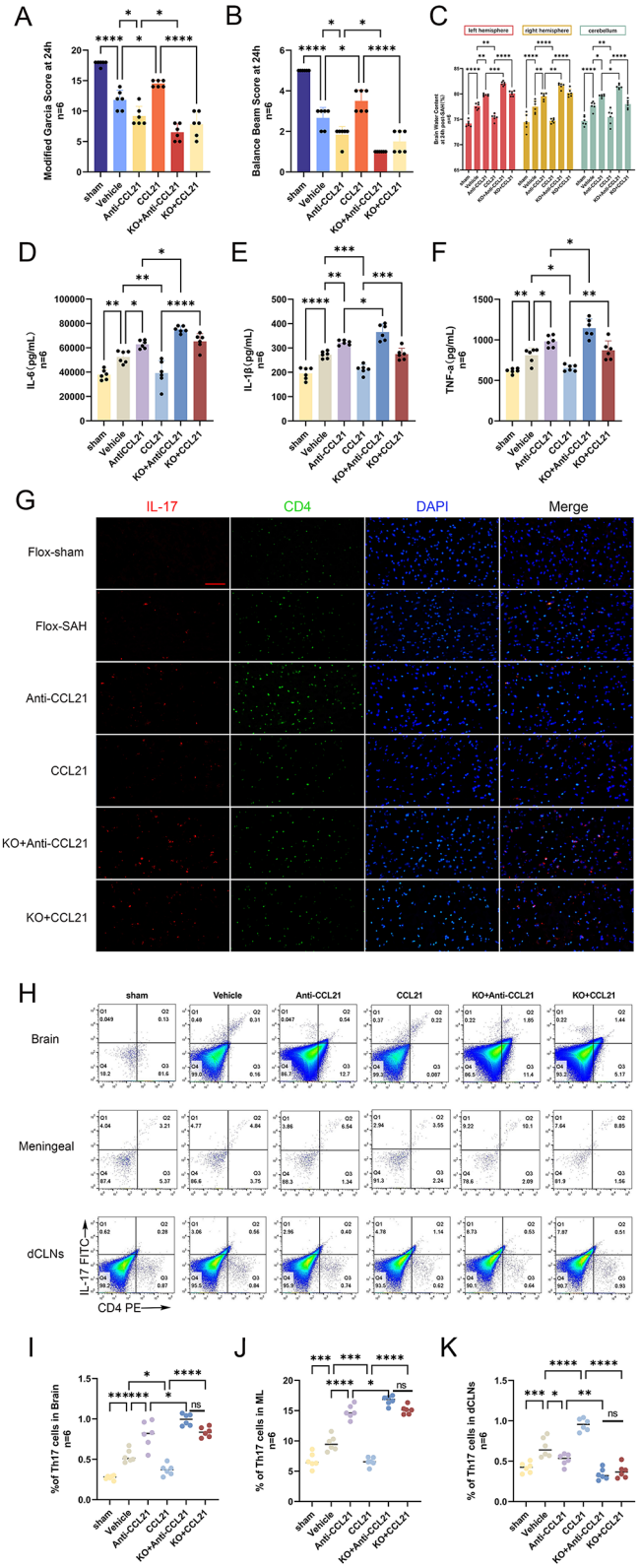

Fig. 7 CCR7-KO exacerbated the neuroinflammation and behavioral defects induced by SAH. **A-B** Neurological Function Scores Garcia and balance beam tests in KO group and Flox group. **C** brain water content in KO and Flox groups. **D-F** ELISA results of IL-6, IL-1β, and TNF-α. **G** Immunofluorescence staining of brain tissue of CD4 and IL-17 (IL-17 red, CD4 green, and DAPI blue; scale bar = 50 μm, $n = 1$). **H** Flow cytometry analysis of Th17 cell counts in brain tissue, meningeal lymphatic vessels, and dCLNs. **I-K** Statistical analysis of Th17 cell counts in each group in brain tissue meningeal and dCLNs. *$P < 0.05$, **$P < 0.01$, ***$P < 0.001$, ****$P < 0.0001$. ns, not significant. Mice in the sham, Vehicle, CCL21, and Anti-CCL21 groups were all Flox genotypes

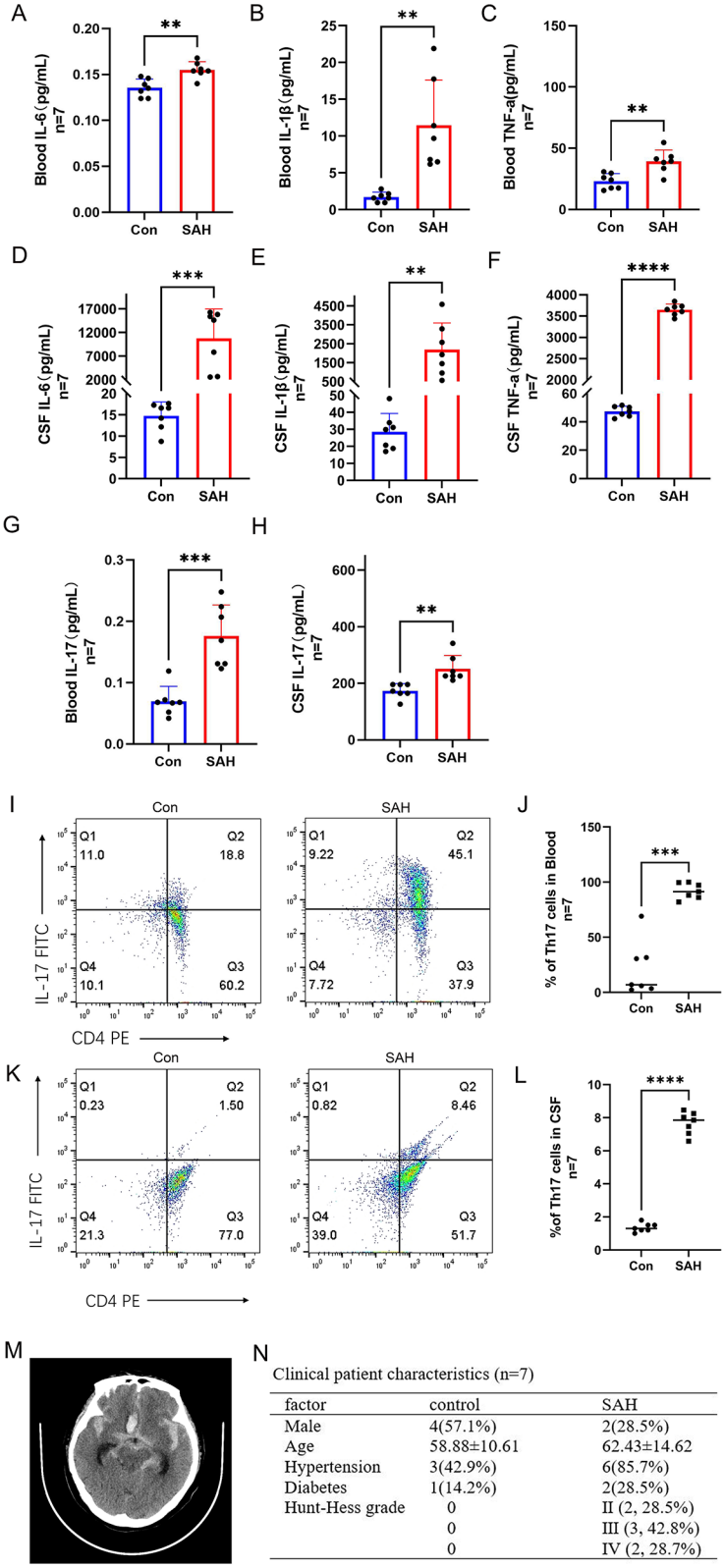

factor	control	SAH
Male	4(57.1%)	2(28.5%)
Age	58.88±10.61	62.43±14.62
Hypertension	3(42.9%)	6(85.7%)
Diabetes	1(14.2%)	2(28.5%)
Hunt-Hess grade	0	II (2, 28.5%)
	0	III (3, 42.8%)
	0	IV (2, 28.7%)

Fig. 8 Neuroinflammatory cytokine levels in blood and cerebrospinal fluid samples from clinical patients after subarachnoid hemorrhage. **A-C** Levels of IL-6, IL-1β, and TNF-α in the blood samples. **D-F** Levels of IL-6, IL-1β, and TNF-α in the CSF samples. **I-L** Flow cytometry analysis the number of Th17 cells in the blood and CSF samples, *$P<0.05$, **$P<0.01$, ***$P<0.001$, ****$P<0.0001$. ns, not significant. **M** CT manifestations of patients with SAH. **N** Clinical patient characteristics ($n=7$)

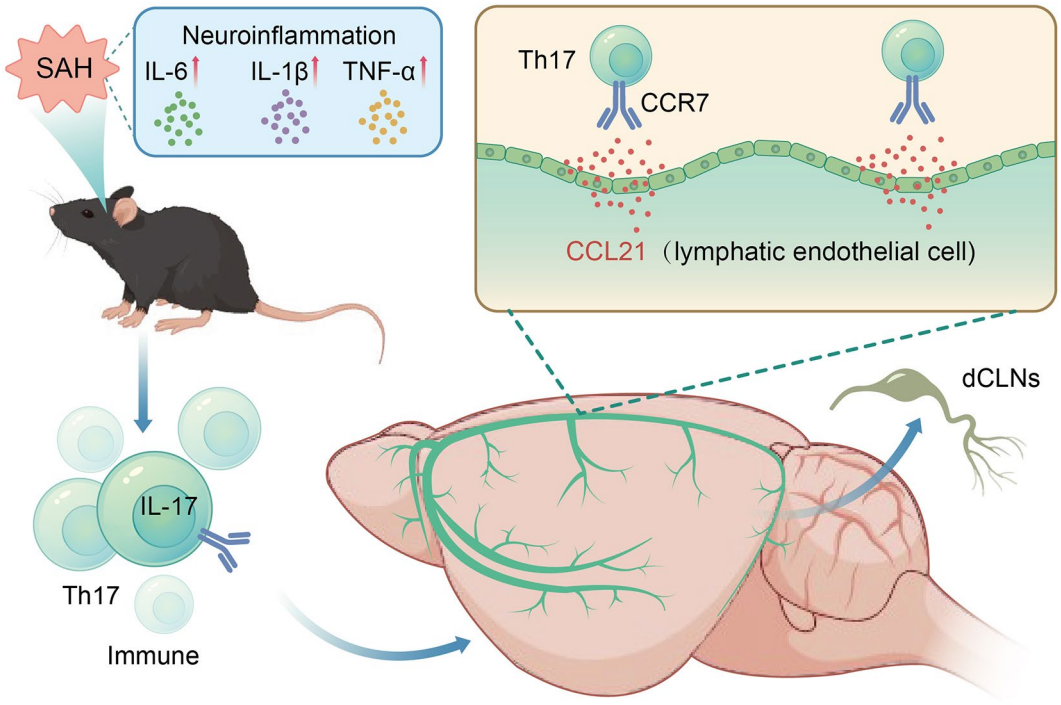

Fig. 9 Mechanism chart

stroke leads to increased concentrations of Th17 cells and IL-17 A in both brain tissue and peripheral blood. In the acute phase, secondary brain injury is triggered by Th17 and IL-17 A, which directly harm neurons, stimulate glial cell activation, disrupt the BBB, and encourage the infiltration of peripheral immune cells [27]. Th17 cells have been demonstrated to have a significant influence on the regulation of the immune system and the body's response to inflammation after SAH, greatly affecting the development of pathophysiology [28]. Under normal conditions, there are almost no immune cells in brain tissue. After SAH, blood enters the subarachnoid space, and the immune system is activated, causing a high infiltration of blood-borne immune cells in the brain parenchyma. Most T cells come from blood infiltrated and extravasated from the brain and are key points in the inflammatory cascade response [15]. Brain tissue is exposed to immune cells and neurotoxic substances, ultimately leading to secondary brain injury; for instance, monocytes and neutrophils further secrete inflammatory cytokines, thereby promoting pro-inflammatory conditions. It can promote the aggregation and activation of neutrophils, thereby exacerbating brain edema and damage. Changes in the BBB after bleeding lead to inflammation and the entry of circulating immune cells into the brain parenchyma, which interact with innate immune cells in the CNS [29]. As described in this article, Th17 cells are found within the intracranial region and CSF and participate in inflammatory responses by producing IL-17, leading to decreased BBB integrity and increased brain edema. Th17 cells exacerbate neuroinflammatory damage after SAH. Administration of an IL-17 monoclonal antibody before SAH induction can alleviate local brain inflammation and improve post-SAH brain edema and brain injury. In 2015, two research teams independently reported discovering evidence of lymphatic vasculature (LV) inside the defensive layers known as meninges that encase the brain and spinal cord of a mouse. This finding contradicted accepted wisdom in the field of neuroimmunology [30, 31]. The meningeal lymphatic system is a series of vasculature situated within the brain parenchyma beneath the meninges and connected to the lymphatic system and CSF [32–34]. The meningeal lymphatic system promotes the transport of immune cells, interstitial fluid, CSF, small chemicals, and subarachnoid space to reach dCLNs [35]. Prox1, a homeobox transcription factor, and VEGFR-3, a vascular endothelial growth factor receptor, play key roles in the process of lymphangiogenesis, according to developments in the research on lymphatic development [36]. Research has successfully shown that Podoplanin (PDPN), CCL21, and Lyve-1 are surface markers for lymphatic endothelial cells (LECs) [37, 38].

The discovery of the role of meningeal lymphatics in clearing immune cells, macromolecules, and CSF has provided insights into the underlying mechanisms of several neurological diseases, such as multiple sclerosis, Alzheimer's disease, brain tumors, and ischemic brain

injury [39]. Meningeal lymphatic drainage abnormalities have been demonstrated in studies to worsen cerebral ischemia and edema following SAH [40]. Research has also demonstrated that following a SAH, red blood cells can be removed by meningeal lymphatic channels [41]. Cervical lymphatic artery ligation slows down blood flow and deteriorates the results of experimental SAH [42]. One open topic is whether immune cells can be cleared by meningeal lymphatics after SAH. Our findings indicate that immune cells that move into the subarachnoid space are transported via the meningeal lymphatic system to the dCLNs. Enhanced lymphatic flow results from enhanced lymphangiogenesis and vascular dilatation in peripheral acute inflammations. Including colitis, bacterial keratitis, and arthritis [43]. Filariasis is a frequent pathological condition resulting from bacterial infection, distinguished by compromised lymphatic transport leading to peripheral lymphedema. The VEGF-C/VEGFR-3 signaling pathway mediates disorders in lymphangiogenesis, affecting local immune responses [44]. Improving the function of lymphatic vessels can alleviate peripheral edema. Localized inflammation and edema are lessened by this rise in lymphatic flow and lymphangiogenesis [43]. Brain edema rapidly develops after SAH and is closely related to BBB destruction. Cerebral edema serves as an independent adverse prognostic indicator for SAH. The development of vascular edema is attributed to endothelial cell dysfunction, the disruption of tight junctions, and the degradation of the basement membrane. Secondly, the toxic substances released from the blood produce cytotoxic edema, which is the second component of brain edema [45]. We alleviated the occurrence of brain edema by overexpressing VEGF-C, while ablation of meningeal lymphatic vessels exacerbated brain edema, showing the crucial role of meningeal lymphatic vessels in draining express water. Delivery of overexpressed VEGF-C locally or via viral infection has proved its efficacy [46]. Blocking the VEGF-C/VEGFR-3 pathway worsens the inflammatory reaction [47, 48]. EAE-related neuroinflammation did not change the architecture of meningeal lymphatic vessels, indicating a restricted ability to expand during neuroinflammation [49]. To confirm the effect of overexpressed VEGF-C or other variables on lymphangiogenesis, more research is needed. T cells and dendritic cells use the pathway involving C-C chemokine motif ligand 21 and C-C chemokine motif receptor 7 to enter and migrate through the peripheral lymphatic system and meningeal lymphatic vessels [50]. The control of immunity in meningeal lymphatic capillaries is greatly aided by the CCR7-CCL21 signaling pathway. CCR7 and CCL21 are key molecules in this pathway. CCR7 is a receptor found mostly on the surface of immune cells, notably dendritic and activated T cells. CCR7 binds to its ligand and then helps these immune cells migrate in a targeted manner to the locations where they mount an immune response. On the other hand, lymphatic tissues and activated endothelial cells normally synthesize CCL21, which functions as a ligand for CCR7. CCL21 is an essential part of the immune system that is responsible for directing immune cells during their migration processes [51]. Deep cervical lymph nodes CCR7 knockdown T cells demonstrated a considerable reduction in drainage when contrasted with wild-type CCR7 T cells. According to Louveau, in steady-state settings, approximately 40% of meningeal $CD4^+$ T cells express the CCR7 receptor during lymphatic drainage of T cells [35]. After SAH, the immune cells and inflammatory mediators caused by bleeding need to be cleared in a timely manner to alleviate brain tissue damage. Enhancing the lymphatic draining function of the meningeal lymphatic through the CCR7-CCL21 axis helps to remove these harmful substances from the CNS. We further confirmed that Th17 cell drainage decreased after knocking out the CCR7 gene. At the same time, it was found that injection of the CCL21 antibody also reduced T cell drainage in the group without CCR7 knockout. These further confirmed that the CCR7-CCL21 pathway plays a crucial function in draining Th17 cells. The limitation of this study was that we used a mouse model to test molecular pathways but lacked human trials. It focused on Th17 cell drainage and neuroinflammation reduction via the CCR7-CCL21 pathway; We have not conducted experiments on other immune cells or pathways. Future research could apply these findings to humans, explore the roles of additional immune cells (e.g., Treg cells) in SAH, and investigate alternative pathways for immune cell modulation.

Conclusion

Our research shows that Th17 cells reach the cervical lymph nodes via the CCR7-CCL21 pathway on the meningeal lymphatics, which reduces inflammation damage after SAH. This enhances our comprehension of the preliminary clearance mechanism for extravasated immune cells in SAH and proposes potential treatments for patients.

Abbreviations

SAH	Subarachnoid hemorrhage
DCI	Delayed brain injury
EBI	Early brain injury
CNS	Central nervous system
CSF	Cerebrospinal fluid
TNF-α	Tumor necrosis factor-α
IL-17	Interleukin-17
IL-6	Interleukin-6
IL-1β	Interleukin-1β
NK cells	Natural killer cells
TGF-β1	Transforming Growth Factor-β1
dCLNs	Deep cervical lymph nodes
MLV	Meningeal lymphatic vessel
Lyve-1	Lymphatic vessel endothelial hyaluronan receptor
VEGFR3	Vascular endothelial growth factor receptor 3

LECs Lymphatic endothelial cells

Author contributions
Dandan Gao: Writing–review and editing, Writing–original draft, Validation, Software, Project administration, Methodology, Investigation, Formal Analysis, Data curation, Conceptualization. Bin Zou, Kunyuan Zhu, Shijun Bi, Wenxu Zhang, Xinyu Yang, Jieyu Lai: Writing–original draft, Investigation. Guobiao Liang: Writing–original draft, Writing–review and editing, Visualization, Validation, Supervision, Resources, Project administration, Funding acquisition, Conceptualization. Pengyu Pan : Writing–original draft, Writing–review and editing, Visualization, Validation, Supervision, Resources, Project administration, Funding acquisition, Conceptualization.

Funding
This work was supported by National Natural Science Foundation of China (Grant Nos. 81971133, 82071481, and 82301487), Liaoning Province "Revitalization Talents Program" (Grant Nos. XLYC2002109), Liaoning Provincial Science and Technology Plan (Grant Nos. 2023JH2/101700096).

Data availability
Data is obtained upon reasonable request from the corresponding author.

Declarations

Ethics approval and consent to participate
All procedures were approved by the Ethics Committee of General hospital of Northern Theater Command (Ethics number: Y (2021) 006, Registration number: ChiCTR2200058298) and followed the principles of Declaration of Helsinki.

Competing interests
The authors declare no competing interests.

Author details
[1]Department of Neurosurgery, General Hospital of Northern Theater Command, 83 Wenhua Road, Shenhe District, Shenyang 110016, China
[2]Department of Aanesthesiology, General Hospital of Northern Theater Command, Shenyang, China
[3]China Medical University, Shenyang, Liaoning, China
[4]Dalian Medical University, Dalian, China

Received: 23 August 2024 / Accepted: 3 October 2024
Published online: 20 October 2024

References

1. Hoh BL, Ko NU, Amin-Hanjani S, Chou S, Cruz-Flores S, Dangayach NS, Derdeyn CP, Du R, Hanggi D, Hetts SW, Ifejika NL, Johnson R, Keigher KM, Leslie-Mazwi TM, Lucke-Wold B, Rabinstein AA, Robicsek SA, Stapleton CJ, Suarez JI, Tjoumakaris SI, Welch BG. 2023 Guideline for the management of patients with Aneurysmal Subarachnoid Hemorrhage: a Guideline from the American Heart Association/American Stroke Association. Stroke. 2023;54(7):e314–70.
2. van Lieshout JH, Dibue-Adjei M, Cornelius JF, Slotty PJ, Schneider T, Restin T, Boogaarts HD, Steiger HJ, Petridis AK, Kamp MA. An introduction to the pathophysiology of aneurysmal subarachnoid hemorrhage. Neurosurg Rev. 2018;41(4):917–30.
3. Mashaly HA, Provencio JJ. Inflammation as a link between brain injury and heart damage: the model of subarachnoid hemorrhage. Cleve Clin J Med. 2008;75(Suppl 2):S26–30.
4. Jin J, Duan J, Du L, Xing W, Peng X, Zhao Q. Inflammation and immune cell abnormalities in intracranial aneurysm subarachnoid hemorrhage (SAH): relevant signaling pathways and therapeutic strategies. Front Immunol. 2022;13:1027756.
5. Brait VH, Arumugam TV, Drummond GR, Sobey CG. Importance of T lymphocytes in brain injury, immunodeficiency, and recovery after cerebral ischemia. J Cereb Blood Flow Metab. 2012;32(4):598–611.
6. Zheng Zou YDDL, Xu G, Peng-Yu GL, Pan. MAP4K4 induces early blood-brain barrier damage in a murine subarachnoid hemorrhage model. Neural regeneration research; 2021.
7. Tamassia N, Bianchetto-Aguilera F, Arruda-Silva F, Gardiman E, Gasperini S, Calzetti F, Cassatella MA. Cytokine production by human neutrophils: revisiting the dark side of the moon. Eur J Clin Invest. 2018;48(Suppl 2):e12952.
8. Miossec P. Diseases that may benefit from manipulating the Th17 pathway. Eur J Immunol. 2009;39(3):667–9.
9. Turner MD, Nedjai B, Hurst T, Pennington DJ. Cytokines and chemokines: at the crossroads of cell signalling and inflammatory disease. Biochim Biophys Acta. 2014;1843(11):2563–82.
10. Kebir H, Kreymborg K, Ifergan I, Dodelet-Devillers A, Cayrol R, Bernard M, Giuliani F, Arbour N, Becher B, Prat A. Human TH17 lymphocytes promote blood-brain barrier disruption and central nervous system inflammation. Nat Med. 2007;13(10):1173–5.
11. Okada T, Suzuki H. Mechanisms of neuroinflammation and inflammatory mediators involved in brain injury following subarachnoid hemorrhage. Histol Histopathol. 2020;35(7):623–36.
12. Louveau A, Herz J, Alme MN, Salvador AF, Dong MQ, Viar KE, Herod SG, Knopp J, Setliff JC, Lupi AL, Da MS, Frost EL, Gaultier A, Harris TH, Cao R, Hu S, Lukens JR, Smirnov I, Overall CC, Oliver G, Kipnis J. CNS lymphatic drainage and neuroinflammation are regulated by meningeal lymphatic vasculature. Nat Neurosci. 2018;21(10):1380–91.
13. Pan P, Zhao H, Zhang X, Li Q, Qu J, Zuo S, Yang F, Liang G, Zhang JH, Liu X, He H, Feng H, Chen Y. Cyclophilin a signaling induces pericyte-associated blood-brain barrier disruption after subarachnoid hemorrhage. J Neuroinflammation. 2020;17(1):16.
14. Tsai HH, Hsieh YC, Lin JS, Kuo ZT, Ho CY, Chen CH, Chang CF. Functional Investigation of Meningeal Lymphatic System in Experimental Intracerebral Hemorrhage. Stroke. 2022;53(3):987–98.
15. Shi SX, Xiu Y, Li Y, Yuan M, Shi K, Liu Q, Wang X, Jin WN. CD4(+) T cells aggravate hemorrhagic brain injury. Sci Adv. 2023;9(23):eabq0712.
16. Eric S, Mao TY, Dong HP, Ligia S, Salli A, Marcus B, Kari A, Thomas JL, Akiko I. VEGF-C-driven lymphatic drainage enables brain tumor immunosurveillance. Nature. 2020;577(7792):689–94.
17. Chen H, Xu C, Zeng H, Zhang Z, Wang N, Guo Y, Zheng Y, Xia S, Zhou H, Yu X, Fu X, Tang T, Wu X, Chen Z, Peng Y, Cai J, Li J, Yan F, Gu C, Chen G, Chen J. Ly6C-high monocytes alleviate brain injury in experimental subarachnoid hemorrhage in mice. J Neuroinflammation. 2023;20(1):270.
18. Xie Y, Guo H, Wang L, Xu L, Zhang X, Yu L, Liu Q, Li Y, Zhao N, Zhao N, Ye R, Liu X. Human albumin attenuates excessive innate immunity via inhibition of microglial Mincle/Syk signaling in subarachnoid hemorrhage. Brain Behav Immun. 2017;60:346–60.
19. Schneider UC, Xu R, Vajkoczy P. Inflammatory events following subarachnoid hemorrhage (SAH). Curr Neuropharmacol. 2018;16(9):1385–95.
20. Geraghty JR, Lung TJ, Hirsch Y, Katz EA, Cheng T, Saini NS, Pandey DK, Testai FD. Systemic Immune-inflammation index predicts delayed cerebral vasospasm after Aneurysmal Subarachnoid Hemorrhage. Neurosurgery. 2021;89(6):1071–9.
21. Heppner FL, Greter M, Marino D, Falsig J, Raivich G, Hovelmeyer N, Waisman A, Rulicke T, Prinz M, Priller J, Becher B, Aguzzi A. Experimental autoimmune encephalomyelitis repressed by microglial paralysis. Nat Med. 2005;11(2):146–52.
22. Zhang HF, Zhao MG, Liang GB, Yu CY, He W, Li ZQ, Gao X. Dysregulation of CD4(+) T cell subsets in intracranial aneurysm. DNA Cell Biol. 2016;35(2):96–103.
23. Mracsko E, Javidi E, Na SY, Kahn A, Liesz A, Veltkamp R. Leukocyte invasion of the brain after experimental intracerebral hemorrhage in mice. Stroke. 2014;45(7):2107–14.
24. Liu H, Pan W, Tang C, Tang Y, Wu H, Yoshimura A, Deng Y, He N, Li S. The methods and advances of adaptive immune receptors repertoire sequencing. Theranostics. 2021;11(18):8945–63.
25. Hughes JT, Schianchi PM. Cerebral artery spasm. A histological study at necropsy of the blood vessels in cases of subarachnoid hemorrhage. J Neurosurg. 1978;48(4):515–25.
26. Moraes L, Trias N, Brugnini A, Grille P, Lens D, Biestro A, Grille S. TH17/Treg imbalance and IL-17A increase after severe aneurysmal subarachnoid hemorrhage. J Neuroimmunol. 2020;346:577310.
27. Wang J, Gao Y, Yuan Y, Wang H, Wang Z, Zhang X. Th17 cells and IL-17A in ischemic stroke. Mol Neurobiol. 2024;61(4):2411–29.
28. Fouser LA, Wright JF, Dunussi-Joannopoulos K, Collins M. Th17 cytokines and their emerging roles in inflammation and autoimmunity. Immunol Rev. 2008;226:87–102.

29. Cheng X, Ye J, Zhang X, Meng K. Longitudinal variations of CDC42 in patients with Acute Ischemic Stroke during 3-Year period: correlation with CD4(+) T cells, Disease Severity, and prognosis. Front Neurol. 2022;13:848933.
30. Secker GA, Harvey NL. VEGFR signaling during lymphatic vascular development: from progenitor cells to functional vessels. Dev Dyn. 2015;244(3):323–31.
31. Aspelund A, Antila S, Proulx ST, Karlsen TV, Karaman S, Detmar M, Wiig H, Alitalo K. A dural lymphatic vascular system that drains brain interstitial fluid and macromolecules. J Exp Med. 2015;212(7):991–9.
32. Ahn JH, Cho H, Kim JH, Kim SH, Ham JS, Park I, Suh SH, Hong SP, Song JH, Hong YK, Jeong Y, Park SH, Koh GY. Meningeal lymphatic vessels at the skull base drain cerebrospinal fluid. Nature. 2019;572(7767):62–6.
33. Louveau A, Da MS, Kipnis J. Lymphatics in Neurological disorders: a neuro-lympho-vascular component of multiple sclerosis and Alzheimer's Disease? Neuron. 2016;91(5):957–73.
34. Bielecki B, Jatczak-Pawlik I, Wolinski P, Bednarek A, Glabinski A. Central Nervous System and Peripheral expression of CCL19, CCL21 and their receptor CCR7 in experimental model of multiple sclerosis. Arch Immunol Ther Exp (Warsz). 2015;63(5):367–76.
35. Louveau A, Smirnov I, Keyes TJ, Eccles JD, Rouhani SJ, Peske JD, Derecki NC, Castle D, Mandell JW, Lee KS, Harris TH, Kipnis J. Structural and functional features of central nervous system lymphatic vessels. Nature. 2015;523(7560):337–41.
36. Srinivasan RS, Escobedo N, Yang Y, Interiano A, Dillard ME, Finkelstein D, Mukatira S, Gil HJ, Nurmi H, Alitalo K, Oliver G. The Prox1-Vegfr3 feedback loop maintains the identity and the number of lymphatic endothelial cell progenitors. Genes Dev. 2014;28(19):2175–87.
37. Petrova TV, Koh GY. Biological functions of lymphatic vessels. Science, 2020. 369(6500).
38. Da MS, Louveau A, Vaccari A, Smirnov I, Cornelison RC, Kingsmore KM, Contarino C, Onengut-Gumuscu S, Farber E, Raper D, Viar KE, Powell RD, Baker W, Dabhi N, Bai R, Cao R, Hu S, Rich SS, Munson JM, Lopes MB, Overall CC, Acton ST, Kipnis J. Functional aspects of meningeal lymphatics in ageing and Alzheimer's disease. Nature. 2018;560(7717):185–91.
39. Hu X, Deng Q, Ma L, Li Q, Chen Y, Liao Y, Zhou F, Zhang C, Shao L, Feng J, He T, Ning W, Kong Y, Huo Y, He A, Liu B, Zhang J, Adams R, He Y, Tang F, Bian X, Luo J. Meningeal lymphatic vessels regulate brain tumor drainage and immunity. Cell Res. 2020;30(3):229–43.
40. Pu T, Wenyan Z, Weixi F, Yanli Z, Wang L, Hongxing W, Xiao AM. Persistent malfunction of Glymphatic and meningeal lymphatic drainage in a mouse model of subarachnoid hemorrhage. Experimental Neurobiol. 2019;28(1):104–18.
41. Chen J, Wang L, Xu H, Xing L, Zhuang Z, Zheng Y, Li X, Wang C, Chen S, Guo Z, Liang Q, Wang Y. Meningeal lymphatics clear erythrocytes that arise from subarachnoid hemorrhage. Nat Commun. 2020;11(1):3159.
42. Luo SQ, Gao SQ, Fei MX, Xue-Wang Y-S, Ran-Zhao YL, Han HD, Wang, Zhou ML. Ligation of cervical lymphatic vessels decelerates blood clearance and worsens outcomes after experimental subarachnoid hemorrhage. Brain Res. 2024;1837:148855.
43. Van Raemdonck K, Umar S, Shahrara S. The pathogenic importance of CCL21 and CCR7 in rheumatoid arthritis. Cytokine Growth Factor Rev. 2020;55:86–93.
44. Nurlaila I, Roh K, Yeom CH, Kang H, Lee S. Acquired lymphedema: molecular contributors and future directions for developing intervention strategies. Front Pharmacol. 2022;13:873650.
45. Hayman EG, Wessell A, Gerzanich V, Sheth KN, Simard JM. Mechanisms of global cerebral edema formation in Aneurysmal Subarachnoid Hemorrhage. Neurocrit Care. 2017;26(2):301–10.
46. Schwager S, Detmar M. Inflammation and lymphatic function. Front Immunol. 2019;10:308.
47. Hsu M, Rayasam A, Kijak JA, Choi YH, Harding JS, Marcus SA, Karpus WJ, Sandor M, Fabry Z. Neuroinflammation-induced lymphangiogenesis near the cribriform plate contributes to drainage of CNS-derived antigens and immune cells. Nat Commun. 2019;10(1):229.
48. Xu JQ, Liu QQ, Huang SY, Duan CY, Lu HB, Cao Y, Hu JZ. The lymphatic system: a therapeutic target for central nervous system disorders. Neural Regen Res. 2023;18(6):1249–56.
49. Liu R, Du S, Zhao L, Jain S, Sahay K, Rizvanov A, Lezhnyova V, Khaibullin T, Martynova E, Khaiboullina S, Baranwal M. Autoreactive lymphocytes in multiple sclerosis: Pathogenesis and treatment target. Front Immunol. 2022;13:996469.
50. Weber M, Hauschild R, Schwarz J, Moussion C, de Vries I, Legler DF, Luther SA, Bollenbach T, Sixt M. Interstitial dendritic cell guidance by haptotactic chemokine gradients. Science. 2013;339(6117):328–32.
51. Geraldo LH, Garcia C, Xu Y, Leser FS, Grimaldi I, de Camargo ME, Dejaegher J, Solie L, Pereira CM, Correia AH, De Vleeschouwer S, Tavitian B, Canedo N, Mathivet T, Thomas JL, Eichmann A, Lima F. CCL21-CCR7 signaling promotes microglia/macrophage recruitment and chemotherapy resistance in glioblastoma. Cell Mol Life Sci. 2023;80(7):179.

Publisher's note